

pubs.acs.org/acschemicalbiology Articles

# Hematoxylin Nuclear Stain Reports Oxidative Stress via Near-Infrared Emission

Rachel E. Langenbacher, Christopher P. Horoszko, Mijin Kim, and Daniel A. Heller\*



Cite This: ACS Chem. Biol. 2023, 18, 1237-1245



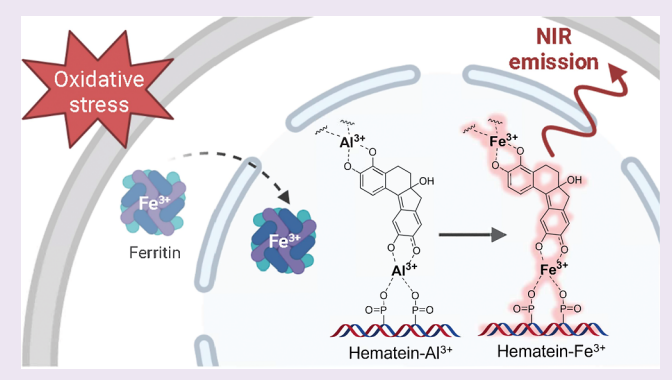
**ACCESS** I

III Metrics & More

Article Recommendations

Supporting Information

ABSTRACT: Hematoxylin & eosin (H&E) is the gold standard histological stain used for medical diagnosis and has been used for over a century. Herein, we examined the near-infrared II (NIR-II) fluorescence of this stain. We observed significant NIR-II emission from the hematoxylin component of the H&E stain. We found that the emission intensity, using the common aluminum(III) hematoxylin mordant, could be modulated by the availability of endogenous iron(III), and this emission intensity increased at higher oxidative stress. Our mechanistic investigations found that hematoxylin emission reported the nuclear translocation of the iron via the protein ferritin. In human tumor tissue samples, oxidative stress biomarkers correlated with hematoxylin NIR-II emission intensity. Emission response of the stain was also observed in



human Alzheimer's disease brain tissue regions affected by disease progression, suggesting that ferritin nuclear translocation is preserved in these regions as an oxidative stress response. These findings indicate that NIR-II emission from the H&E stain provides a new source of redox information in tissues with implications for biomedical research and clinical practice.

# **■ INTRODUCTION**

The hematoxylin and eosin (H&E) stain is the most widely used histological technique in laboratory medicine. H&E staining produces deep blue coloring of nuclei by hematoxylin and pink coloring of the cytoplasm and extracellular matrix by eosin. H&E provides contrast for morphological assessment and is commonly used for this purpose in the diagnosis of many diseases. The preparation and processing of H&E-stained samples require experienced, well-trained personnel, and because assessment is still carried out by the naked eye, all interpretations carry a degree of subjectivity. Increasing interest and demand exist for technical advances that can produce more objective results at lower costs and mine additional, clinically relevant data from stained samples.

The hematoxylin component of this stain requires the use of a mordant, a redox-active metal, in order to produce stable dye complexes with nuclear chromatin.<sup>3</sup> For H&E, aluminum in the form of Al(III) is typically used as a mordant, although iron, Fe(III), also produces nuclear staining and is used in other staining protocols.<sup>3</sup> It is also feasible that endogenous metals may serve as additional mordants if they are available in the nucleus, complexing with the hematoxylin stain in addition to the original mordant. For example, in cells, ferritin is reported to translocate to the nucleus under a broad range of oxidative stress conditions when free radicals are present in the nucleus.<sup>4</sup> Nuclear ferritin protects against iron-induced oxidative damage to the DNA by sequestering free iron, Fe(II), in the Fe(III) form.<sup>4</sup> As ferritin may store over 4000

Fe(III) cations per protein,<sup>4</sup> this process greatly increases the nuclear availability of Fe(III) to potentially serve as an additional mordant to the hematoxylin stain.

Clinically, NIR imaging is currently under exploration in surgical settings, <sup>5</sup> but it has been explored less for histopathology. While tissues exhibit significant autofluorescence and absorbance in visible wavelengths, <sup>6</sup> the NIR optical windows can greatly improve signal-to-noise ratios for fluorescence imaging. <sup>2,7</sup> Characterization of fluorescence emission from H&E-stained samples has focused on the visible and NIR-I wavelengths below 900 nm. <sup>8</sup> While eosin fluoresces at around 550 nm, <sup>9</sup> hematoxylin has been reported to lack fluorescence. <sup>2</sup>

In this work, we used NIR hyperspectral microscopy<sup>10,11</sup> to examine the near-infrared II (NIR-II) emission from H&E-stained sections in the 900–1400 nm range under 730 nm excitation, and found a previously undescribed emission signature from H&E-stained samples. The spatially resolved NIR emission originated from nuclei, suggesting that the NIR fluorescence is from hematoxylin. This emission was

Received: March 16, 2023 Accepted: April 5, 2023 Published: April 18, 2023





responsive to the mordant used to complex the hematoxylin dye to the sample and the sample's oxidative stress due to the relevance of nuclear iron. Al(III) hematoxylin emission was significantly dimmer compared to Fe(III) hematoxylin emission. The emission of Al(III) hematoxylin was responsive to manipulation of endogenous iron levels, most probably due to endogenous iron serving as an additional mordant to the Al(III) hematoxylin stain. The Al(III) hematoxylin emission was higher under oxidative stress conditions. Our mechanistic investigations indicated that the emission modulation resulted from the nuclear translocation of iron via the iron transport protein ferritin. To characterize the behavior of this new NIR property of hematoxylin, we investigated oxidative stress via H<sub>2</sub>O<sub>2</sub> treatment of cultured cells. The NIR emission can be abrogated by pharmacological or genetic inhibition of ferritin. Furthermore, the hematoxylin emission changes were distinct and measurable in human tissues. In human tumor tissue samples, the oxidative stress biomarker, superoxide dismutase-1 (SOD-1), correlated with hematoxylin emission intensity. Emission of the stain was also observed in Alzheimer's disease (AD) brain tissue regions affected by disease progression, suggesting that ferritin nuclear translocation is preserved in these regions as an oxidation stress response. Our work demonstrates the potential of NIR-II emission from the H&E stain to quantify oxidative stress in cells and tissues.

#### **■ EXPERIMENTAL SECTION**

**Cell Culture.** HEK293 cells were obtained from the Antibody and Bioresource Core Facility at Memorial Sloan Kettering Cancer Center. Cells were maintained in humidified incubators at 5% CO<sub>2</sub>, 37 °C in Dulbecco's modified Eagle's media supplemented with 10%  $\nu/\nu$  heat-inactivated fetal bovine serum, 1% penicillin—streptomycin, 1% glutamine, and 2.5% HEPES. All reagents were purchased from Gibco Life Technologies. Cells were trypsinized, washed in phosphate buffered saline, and plated on 35 mm glass-bottom Petri dishes (MatTek). Prior to treatment, cells recovered for 24 h and were used for experiments at 70–80% confluence unless otherwise noted. Following treatments, fixation was performed using ice-cold 70% ethanol followed by incubation at -20 °C for 1 h. Cells were then H&E-stained.

**Pharmacological Treatments.** Iron levels were manipulated by treating cells with deferoxamine mesylate (DFO) or ferric ammonium citrate (FAC) as described by Surguladze et al. <sup>12</sup> Briefly, cells were treated with DFO (DFO salt, powder >92.5% TLC, Sigma-Aldrich D9533-1G) to a final concentration of 100  $\mu$ M, incubated for 24 h, washed, and then fixed prior to staining. FAC (PharmaGrade Sigma-Aldrich, RES20400-A702X) was dissolved in sterile deionized H<sub>2</sub>O and diluted in media to a final concentration of 0.1 mM, incubated with cells for 24 h, washed, and then fixed prior to staining.

Oxidative stress was induced in cells with or without drug pretreatment using hydrogen peroxide ( $\rm H_2O_2$ , Sigma-Aldrich 88597-100ML-F), as previously described, <sup>12</sup> added to a final concentration of 30  $\mu$ M. Wheat germ agglutinin (WGA, Sigma-Aldrich L4895-2MG) was added to a final concentration of 0.1 mg/mL 30 min prior to treatment. Importazole (IMP, Sigma-Aldrich, SML0341-5MG) was added to another treatment group to a final concentration of 30  $\mu$ M 1 h prior to  $\rm H_2O_2$  addition. O-glycosylation inhibitors were used as previously described. <sup>4</sup> Briefly, benzyl 2-acetamido-2-deoxy-alpha-D-galactopyranoside (Benzyl- $\alpha$ -GalNAc, Sigma-Aldrich B4894-25MG) was added to a final concentration of 3 mM 1 h prior to  $\rm H_2O_2$  treatment. Alloxan (Alloxan monohydrate 98% Sigma-Aldrich A7413-10G) was added to a final concentration of 1 mM 1 h prior to  $\rm H_2O_2$  treatment.

**Ferritin Knockdown.** Cells were seeded into a 12-well plate, 24 h prior to transfection. Transfection was performed at 30% confluence using ferritin heavy chain shRNA (h) lentiviral particles (Santa Cruz Biotechnology sc-40575-V) according to manufacturer instructions.

Transduced cells were split 1:3, incubated for 24 h, and selected using 5  $\mu$ g/mL puromycin. Knockdown was assessed in treated cells by DAB-IHC staining for ferritin.

Tissue Samples. Alzheimer's Human Multi-tissue Tissue Micro-Array (Novus Biologicals NBP2-78122), Normal Human Brain Tissue Micro-Array (Novus Biologicals NBP2-78063), and Human Multiple Tumor Tissue Micro-Array (Novus Biologicals NBP2-42052) were used to assess hematoxylin signal in diseased and matched control tissues.

Ferritin Staining. The immunofluorescence (IF) detection of ferritin was performed at the Molecular Cytology Core Facility of Memorial Sloan Kettering Cancer Center. Automated IF staining was conducted using Leica Bond BX staining system. Cells cultured on chamber slides were fixed in 4% paraformaldehyde (PFA, Electron Microscopy Sciences, 157-8-100) for 15 min followed by washing in phosphate-buffered saline (PBS). Slides were loaded in Leica Bond, and IF staining was performed as follows. The primary antibodies against FTH1 (Rb, 0.11  $\mu$ g/mL, cell signaling technology, 4393) were incubated with the sample for 1 h at room temperature. After that, the Leica Bond Polymer anti-rabbit HRP secondary antibody [included in Polymer Refine Detection Kit (Leica, DS9800)] was used for 8 min, followed by incubation with Alexa Fluor tyramide signal amplification reagents (Life Technologies, B40953) for 10 min. After the run was finished, slides were washed in PBS and incubated in 5  $\mu$ g/mL 4′, 6diamidino-2-phenylindole (Sigma-Aldrich, D9542) in PBS for 5 min, rinsed in PBS, and mounted in Mowiol 4-88 (Calbiochem). Slides were kept overnight at—20 °C before imaging. The slides were scanned with a 20x/0.8NA objective on a Pannoramic Confocal Scanner (3DHistech, Budapest, Hungary).

**H&E Staining.** Al(III) H&E staining was carried out according to manufacturer's instructions (Vector Laboratories, H&E stain kit H-3502). For Fe(III) H&E staining, FAC (Sigma-Aldrich, RES20400-A702X) was dissolved and mixed in equal molarity with air-aged hematoxylin (hematein) dissolved in deionized water. Air-aged hematoxylin was generated by vigorously shaking the waterhematoxylin solution (Sigma-Aldrich, H9627-25G) daily to aerate the solution over 14 days prior to experimentation. For comparison, hydrogen peroxide (3% v/v, Sigma-Aldrich 88597) was used to chemically cure fresh hematoxylin solution. Mild non-ionic detergent (Tween 20, Fisher Scientific, BP337-100) was used to prevent dye clumping and precipitation in solution. In some cases, ethanol (Fisher Scientific, BP2818500) was added to the dye mixture with or without 4% v/v PFA (32%, Electron Microscopy Sciences, 15714-S). Genomic DNA was extracted from the mouse tail, purified into mild storage buffer, and frozen as stocks before addition into samples.

DAB-IHC Staining. DAB-IHC for SOD-1 was performed with superoxide Dismutase 1 Antibody (NSJ Bioreagents F51318) and mouse anti-rabbit IgG-HRP (Santa Cruz Biotechnology SK-4105). Detection with a DAB kit (ImmPACT DAB HRP Substrate Vector Laboratories SK-4105) was according to manufacturer instructions. Ferritin knockdown was determined by IHC with human ferritin antibody (R&D Systems, mouse monoclonal, MAB93541-SP), goat anti-mouse IgG HRP conjugate (Tonbo Biosciences 72-8042-M001), and ImmPACT DAB HRP substrate. Samples were mounted using 1 part glycerol and 9 parts phosphate buffered saline.

Near-infrared Hyperspectral Fluorescence Microscopy. Near-infrared fluorescence microscopy<sup>11</sup> was used to acquire the spatially and spectrally resolved near-infrared fluorescence emission of fixed and paraffin-sectioned tissue samples. Cover-slipped tissue sections of kidney or lung with and without H&E staining were imaged using the ×50 objective (LCPLN50XIR, NA = 0.65, IR objective, Olympus). The slides were excited with a continuous wave 730 diode laser with an output power of 2 W, homogenized via beam-shaping optics to ensure even illumination across the field of view. The power output at the sample stage was 370.2 mW, corresponding to an irradiance per pixel of 4.38\*10<sup>12</sup> photons. A long-pass dichroic mirror (cut-on wavelength = 775 nm; Semrock) was used to reflect the light source to the Olympus IX-71 microscope outfitted with the objective. Emission was collected with a thermoelectrically cooled two-dimensional (2D) InGaAs array detector (Photon Etc, IMA<sup>TM</sup>)

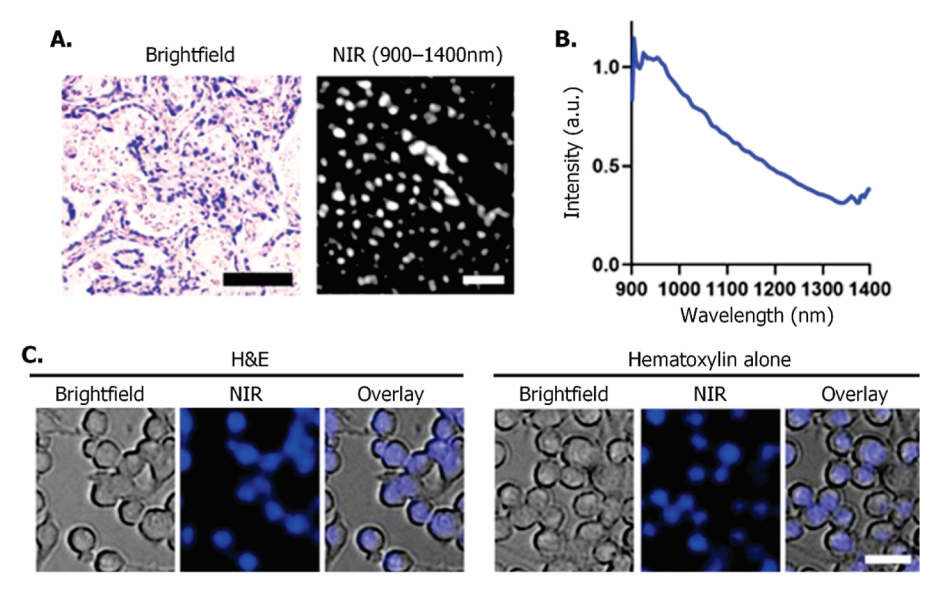


Figure 1. NIR-II emission from H&E-stained tissue and cells. (A) Representative brightfield image (scale bar =  $60 \mu m$ ) and representative NIR image of H&E-stained human kidney tissue section (scale bar =  $30 \mu m$ ). (B) Hyperspectral emission spectrum of 730 nm excited nuclei showing the peak of interest. (C) Brightfield, NIR, and overlay images of H&E-stained cells or cells stained with hematoxylin alone (scale bar =  $20 \mu m$ ).

whose quantum efficiency is over 70% in 870–1600 nm and gain (electrons/ADU) as low as 2.2. Brightfield and broadband near-infrared emission images were obtained under white light illumination and 730 nm excitation (0.2 s exposure), respectively. Hyperspectral microscopy was conducted by passing the emission through a volume Bragg grating placed immediately before the InGaAs array in the optical path. Hyperspectral "cubes" were obtained as previously reported. Data postprocessing, including background subtraction, nonuniformity correction in excitation profile, and wavelength-dependent intensity correction by each pixel, was performed using PHySpec 2.4.1.

Spectral Characterization of Fe(III) Hematoxylin Solutions. Dye-containing solutions were plated into 96 half-well transparent plates (Corning, 3903), and then each sample was briefly vortexed and incubated at room temperature for 5 min, plates were inserted into a multifunctional monochromator-based microplate reader (Tecan, Infinite M1000 Pro) for absorbance and fluorescence readings.

**Statistical Analysis and Software.** Statistical analysis was performed using GraphPad Prism 7. Significance was assessed using one-way ANOVAs performed with a P < 0.05 cutoff. Statistical significance is reported as follows: P < 0.05 = \*, P < 0.01 = \*\*\*, P < 0.001 = \*\*\*, and <math>P < 0.0001 = \*\*\*\*. Image J 1.48 V was used to process NIR broadband images.

# RESULTS AND DISCUSSION

NIR Emission from the Hematoxylin Nuclear Stain. We conducted NIR broadband fluorescence imaging on H&E-stained samples. We used an epifluorescence microscope with an InGaAs array camera sensitive in the 860–1400 nm range to image H&E-stained human kidney samples under 730 nm laser excitation (Figure 1A). Using NIR hyperspectral microscopy, we observed significant emission above 900 nm, to approximately 1350 nm (Figure 1A,B). Upon analysis of fixed HEK293 cells stained with H&E or hematoxylin alone (Figure 1C), we observed that this emission was retained under both staining conditions. This emission was not detected in unstained cells or in cells stained with eosin alone (Figure S1A,B), indicating that the emission originated from the hematoxylin nuclear stain.

NIR-II emission from this stain has not been previously characterized, likely because the CCD and CMOS cameras

used in microscopy over the past three decades are optimized for the 300–850 nm range and exhibit reduced sensitivity toward the upper edge of this range. Additionally, a high excitation power (370.2 mW at 730 nm), such as was used herein, may be required to observe this relatively weak emission. The observed emission is most likely the tail of an emission peak. When emission is captured down to the current instrumental limit of ~784 nm, this tail can more clearly be observed (Figure S2). Due to the low sensitivity of the InGaAs camera under 900 nm, all other NIR imaging experiments presented in the main text use the cutoff of 900 nm. The consistent appearance of this spectral feature in all H&E-stained samples led us to further examine the characteristics of this emission.

Mordant-dependent Spectral Properties of the Hematoxylin Nuclear Stain. We investigated the optical properties of the hematoxylin stain affected by the mordant. Hematoxylin preparations require mordants to form stable associations with cellular material.<sup>3</sup> The hematoxylin component of the H&E stain typically uses Al(III) as a mordant, although other metals such as Fe(III) are also used for staining in some applications. The spectral properties of samples containing Al(III) or Fe(III) mordant were assessed. First, in UV-Vis-NIR absorbance analyses of aqueous hematoxylin solutions, Fe(III) hematoxylin exhibited a different absorbance spectrum as compared to Al(III) hematoxylin (Figure 2A; nonnormalized spectra in Figure S3). The absorbance of Fe(III) hematoxylin increased in the visible and NIR ranges in both the naturally air-ripened and chemically oxidized forms of hematoxylin, and this absorbance further increased in the presence of DNA (Figure S4). Dye absorbance was sensitive to pH; stronger absorbance was found at pH 6 as compared to pH 4, even in the presence of genomic DNA. These results support the hypothesis that hematoxylin-stained tissue forms a photoactive chromogen only near the neutral pH, present after staining and washing. Furthermore, Fe(III) hematoxylin absorbance was largely independent of genomic DNA fixation status (Figure S5). Consistent with this phenomenon, the

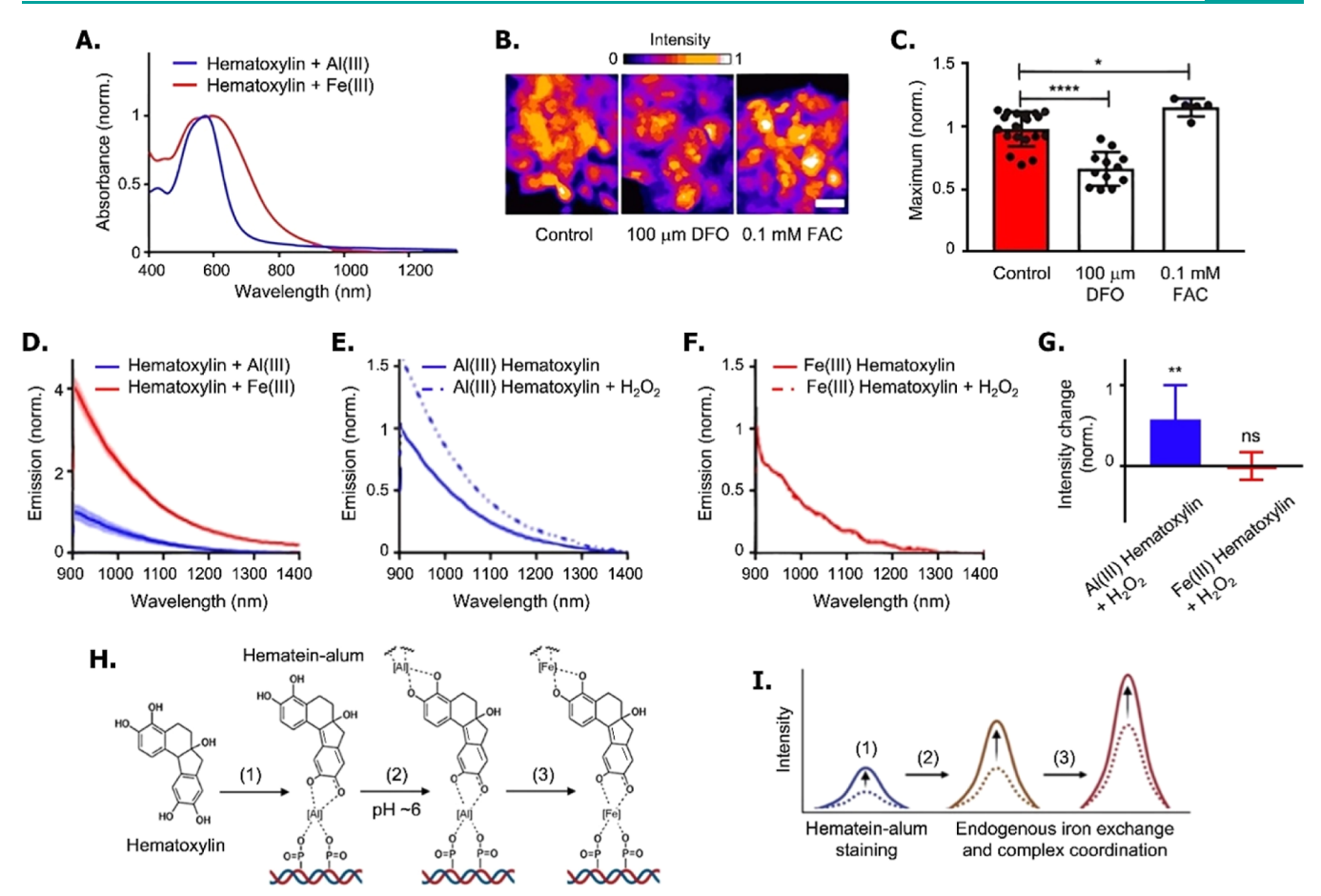


Figure 2. Mordant-dependent spectroscopic dynamics of the hematoxylin stain. (A) Absorbance spectra of Al(III) hematoxylin and Fe(III) hematoxylin in solution. (B) Representative broadband NIR image of control, DFO-treated, and FAC-treated HEK293 cells. (C) Emission intensity from control, DFO-treated, and FAC-treated cells (N = 36; normalized to control). (D) Emission of Al(III) and Fe(III) hematoxylin stained HEK293 cells (normalized to Al(III) hematoxylin) (N = 12). (E) Emission of Al(III) hematoxylin stain in control HEK293 cells and cells treated with 30  $\mu$ M H<sub>2</sub>O<sub>2</sub> (normalized to control). (G) Quantification of intensity changes after H<sub>2</sub>O<sub>2</sub> treatment in HEK293 cells for Al(III) hematoxylin and Fe(III) hematoxylin stains (N = 91). (H) Proposed structure of the hematoxylin-mordant structure. (I) Mordant-dependent changes in absorbance in the visible and NIR ranges. Numbers in parentheses are to correlate the structural changes in hematoxylin to the absorbance/emission band intensity. Dashed and solid line curves indicate the intensity change before and after each treatment condition.

addition of a miscible solvent, ethanol, into the solution ablated dye absorbance (Figure S6).

We next examined whether endogenous iron would affect the spectral properties of Al(III) hematoxylin-stained samples, hypothesizing that hematoxylin may interact with any available mordant-compatible metal cations in addition to the Al(III) mordant. To modulate endogenous iron levels, HEK293 cells were treated with the iron chelator DFO prior to fixation and H&E staining (Figure 2B,C). Hematoxylin emission intensity decreased in these samples. However, upon the addition of the Fe(III) donor FAC in live cells prior to fixation and H&E staining, emission intensity slightly increased (Figure 2C). These results suggest that endogenous iron levels modulated the NIR emission of Al(III) hematoxylin-stained nuclei by increasing emission intensity. This observation was further supported by comparing Al(III) or Fe(III) hematoxylin stain intensity in nuclei upon 730 nm excitation (Figure 2D; nonnormalized spectra in Figure S7A). Al(III) hematoxylin stain intensity was significantly lower than Fe(III).

Given the relationship between cellular iron and oxidative stress, we hypothesized that oxidative stress may induce changes in the spectral properties of Al(III) hematoxylin-

stained samples. Cells were treated with  $H_2O_2$  in order to induce oxidative stress prior to fixing and H&E staining. We found a significant increase in emission from cells stained with Al(III) hematoxylin (Figure 2E; non-normalized graph in Figure S7B). However, the increase in hematoxylin emission from  $H_2O_2$  treatment was not observed when Fe(III) hematoxylin was used (Figure 2F,G).

Based on the abovementioned data, we hypothesize that the coordination of hematoxylin in DNA generates the optical response in the NIR optical window that is enhanced by iron exchange with Al(III) hematoxylin (Figure 2H,I). The response is likely not due to direct oxidative damage, since the Fe(III) mordant is a stronger chromogen as compared to Al(III). This sensitivity to one metal cation over another is not unprecedented; metal ions are reported to induce fluorescence in non-emissive compounds; alternatively, fluorescent compounds may serve as sensors to specific metal cations via specific and significant red-shifting or intensity changes of existing fluorescence. <sup>13,14</sup> Metal sensing by chromophores is described as specific and sensitive due to structure and selective binding. <sup>15,16</sup> Therefore, enhancement of hematoxylin emission in the presence of Fe(III) suggests that the Al(III)

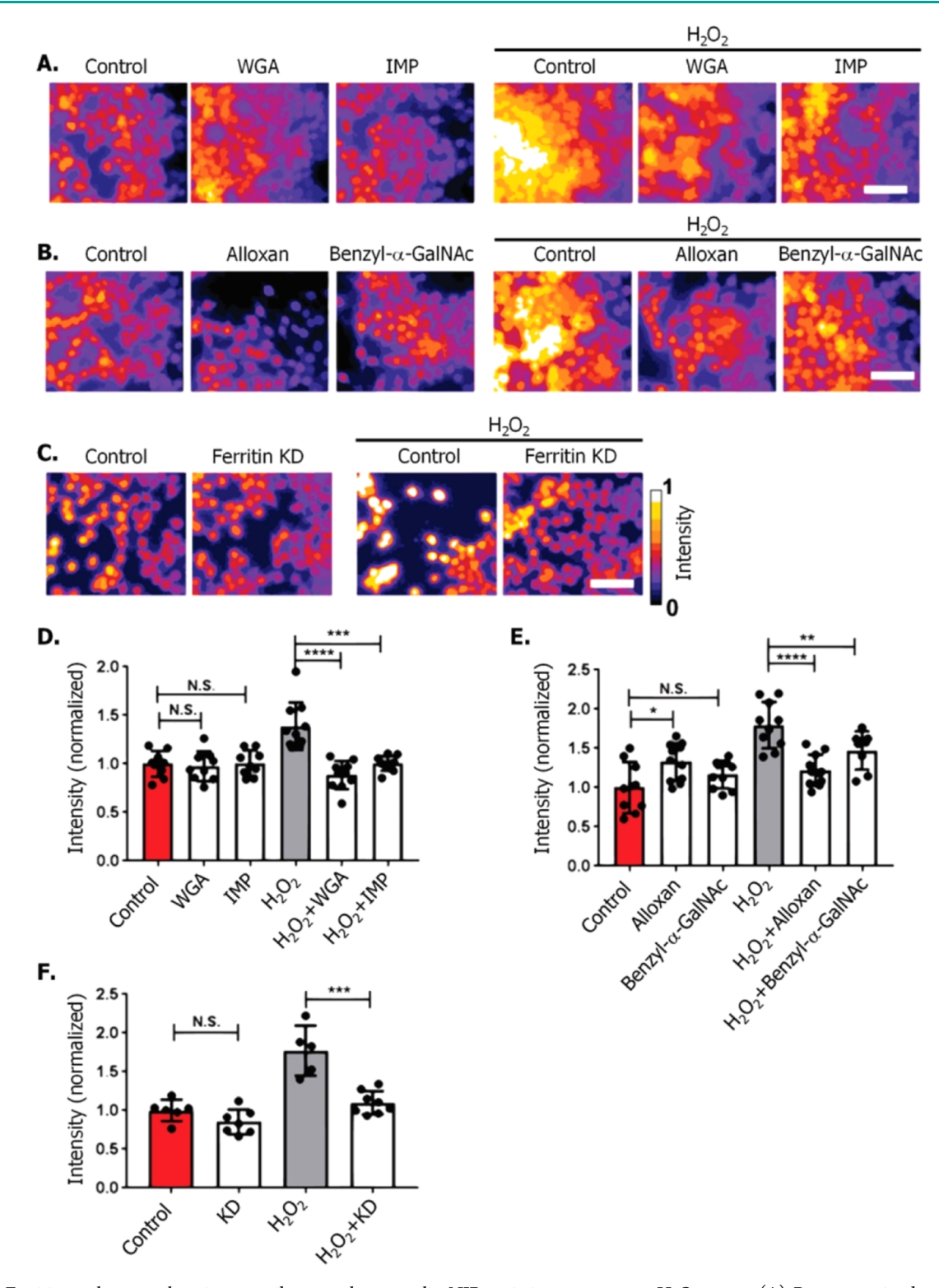


Figure 3. Ferritin nuclear translocation contributes to hematoxylin NIR emission response to  $H_2O_2$  stress. (A) Representative broadband NIR images, with false-color added, of hematoxylin NIR emission intensity from cells treated with vehicle or  $H_2O_2$  with or without addition of WGA or IMP (scale bar = 30 μm). (B) Representative false-color images of hematoxylin NIR emission intensity from cells treated with vehicle or  $H_2O_2$  after pretreatment with Alloxan or Benzyl-α-GalNAc (scale bar = 30 μm). (C) Representative false-color images of hematoxylin NIR emission intensity from cells treated with vehicle or  $H_2O_2$  following ferritin KD; scale bar = 30 μm. (D) Average hematoxylin stain intensity after inhibition of nuclear translocation in  $H_2O_2$ -stressed HEK293 cells (N = 57) (normalized to control). (E) Average hematoxylin stain intensity after ferritin KD in  $H_2O_2$ -stressed HEK293 cells (N = 60; normalized to control). (F) Average hematoxylin stain intensity after ferritin KD in  $H_2O_2$ -stressed HEK293 cells (N = 26; normalized to control).

hematoxylin stain typically used in H&E assays is readily disturbed by levels of Fe(III) in the sample. Endogenous

Fe(III) may serve as an additional mordant to the hematoxylin component of the Al(III) hematoxylin stain. Additional studies

on the nature of oxidative stress-related responses are described below.

Role of Ferritin Nuclear Translocation in Al(III) Hematoxylin-Mediated NIR Response to H<sub>2</sub>O<sub>2</sub>-Induced Oxidation Stress. We assessed whether nuclear ferritin translocation might contribute to hematoxylin emission changes through its iron carrier role. We pharmacologically inhibited nuclear translocation with WGA or IMP treatments with or without  $H_2O_2$  treatment (Figure 3A–D). Pretreatment with either WGA or IMP attenuated the hematoxylin emission response to H2O2 treatment, while treatment with either inhibitor in the absence of oxidative stress did not. Because WGA and IMP are non-selective nuclear trafficking inhibitors, we also examined O-glycosylation, a process that accompanies the transfer of ferritin from the cytoplasm to the nucleus.<sup>4</sup> Pretreatment with either alloxan or benzyl- $\alpha$ -GalNAc, potent inhibitors of O-glycosylation, attenuated the hematoxylin emission response to H<sub>2</sub>O<sub>2</sub> treatment, again, while treatment with either inhibitor in the absence of H<sub>2</sub>O<sub>2</sub> treatment did not attenuate the hematoxylin emission (Figure 3B-E). IF staining of ferritin confirmed that the change in the ratio of nuclear to cytoplasmic ferritin levels was consistent with that observed via the hematoxylin emission response (Figure S8). Nuclear ferritin levels increased via oxidative stress. The ratio of nuclear to cytoplasmic ferritin level was significantly reduced by pretreatment of alloxan in the absence of H<sub>2</sub>O<sub>2</sub> treatment. Under H<sub>2</sub>O<sub>2</sub>-induced oxidative stress, the nuclear ferritin level in alloxan-treated cells was lower than in the control group. These data are consistent with the hypothesis that ferritin nuclear translocation produces hematoxylin NIR optical modulation. However, these pharmacological treatments are not specific to ferritin alone and broadly inhibit nuclear transport and O-glycosylation. Therefore, we performed an shRNA knockdown of ferritin in HEK293 cells to assess whether ferritin nuclear translocation alone produced these spectral changes in hematoxylin emission. When ferritin protein was knocked down, we observed an attenuated hematoxylin spectral response to oxidative stress (Figures 3F

These results are consistent with ferritin's role as the major iron sequestration and transport protein. Ferritin can store thousands of Fe(III) cations per protein,  $^4$  and thus, the nuclear translocation of ferritin under oxidative stress is expected to greatly increase the nuclear availability of Fe(III) to the hematoxylin stain. Taken together, these results indicate that ferritin translocation to the nucleus increases Al(III) hematoxylin NIR emission intensity in response to  $H_2O_2$ -induced oxidative stress, likely through increasing the local concentration of Fe(III) available to serve as an additional mordant to the hematoxylin stain (Figure 4).

Hematoxylin NIR Emission as a Reporter of Oxidative Stress in Clinical Samples. To explore the relationship between oxidative stress and hematoxylin stain emission in diseased clinical samples, we probed hematoxylin emission in human cancer tissues. In human tumor samples counterstained for the oxidative stress marker SOD-1 (Figure 5A), we found that elevated SOD-1 expression correlated with higher hematoxylin NIR emission in comparison to healthy matched controls (Figure 5B,C). These results were consistent with hematoxylin NIR emission reporting oxidative stress in these samples.

Next, we assessed hematoxylin stain NIR emission in human brain samples from AD and matched healthy controls. We

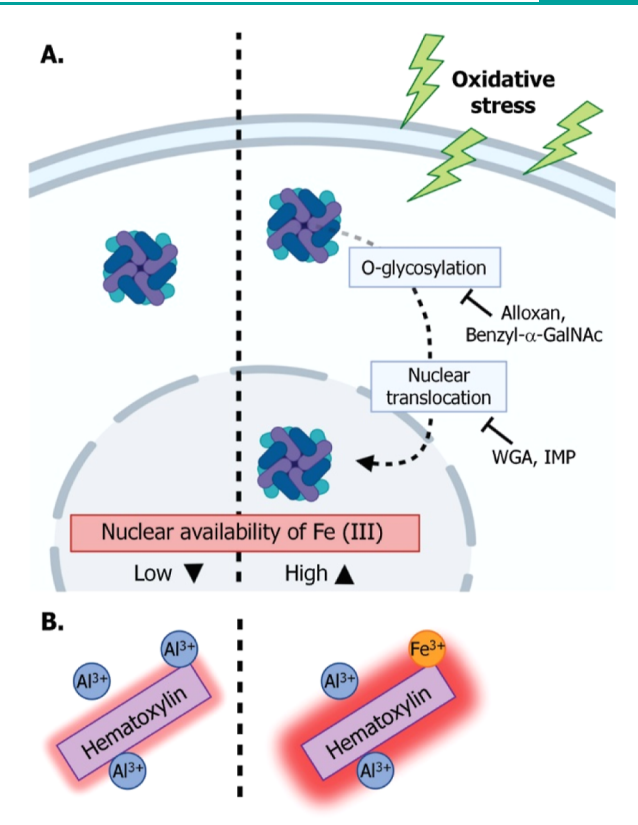


**Figure 4.** Proposed mechanism of hematoxylin NIR response to oxidative stress. (A) Ferritin translocation transports Fe(III) to the nucleus. (B) Fe(III) in the nucleus contributes to the Al(III) hematoxylin emission response.

found that in AD samples, three brain regions showed elevated hematoxylin emission compared to matched healthy controls: the temporal lobe, the parietal lobe, and the frontal lobe (Figure 6A,B).

While microarrays provide a limited sample of tissue that may not be entirely representative of the entire brain region, or of disease as heterogeneous as AD, these anatomical brain areas are reported to contribute to AD etiology. 17-19 Moreover, our data suggest that ferritin nuclear translocation, a biological response to oxidative stress, may be occurring in these brain regions. This finding was somewhat surprising, as other notable oxidative stress responses such as SOD-1 expression are reported to be downregulated during AD progression. 20,21 Despite our observation of AD-associated nuclear-translocation of ferritin in disease-relevant brain regions, the role of ferritin as a potential contributor to AD progression, or a protective response, is not well understood.<sup>22</sup> However, these observations of hematoxylin emission in these samples suggest that in brain regions typically impacted by AD progression, ferritin nuclear translocation may be preserved, which would be consistent with ferritin having a potential protective role against oxidative stress in AD.

Together, these data suggest that the NIR properties of the hematoxylin stain may have clinical utility, providing a readout of oxidative stress in diseased states. Oxidative stress is important to both disease progression and the effective treatment of human cancers.<sup>23</sup> Because increased nuclear ferritin is reported to decrease the efficacy of chemotherapeutics such as cisplatin,<sup>24</sup> this hematoxylin spectral response may be of use to direct effective treatments. In AD

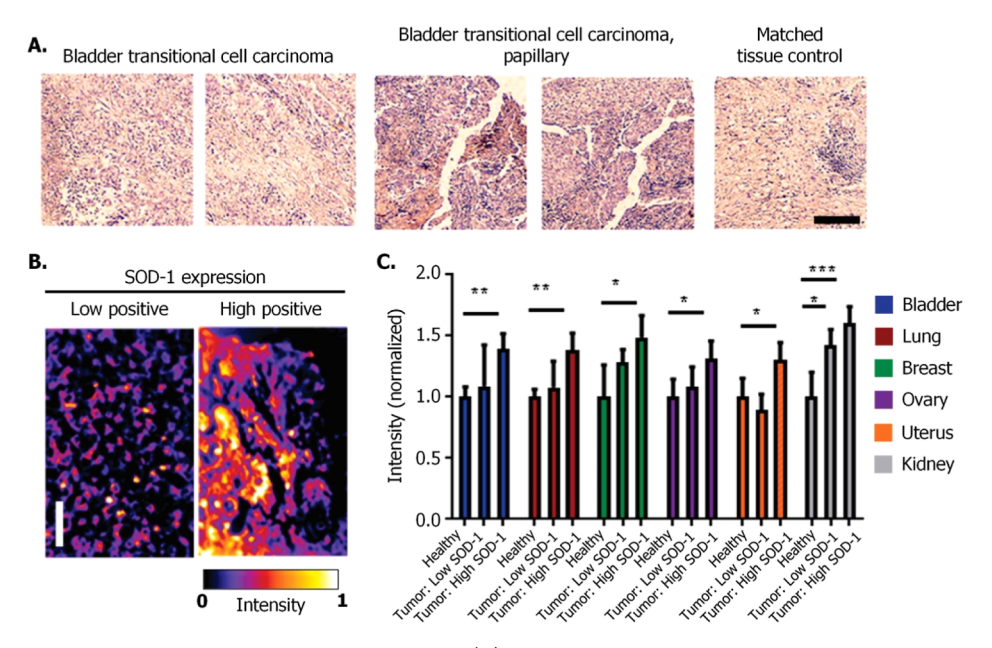
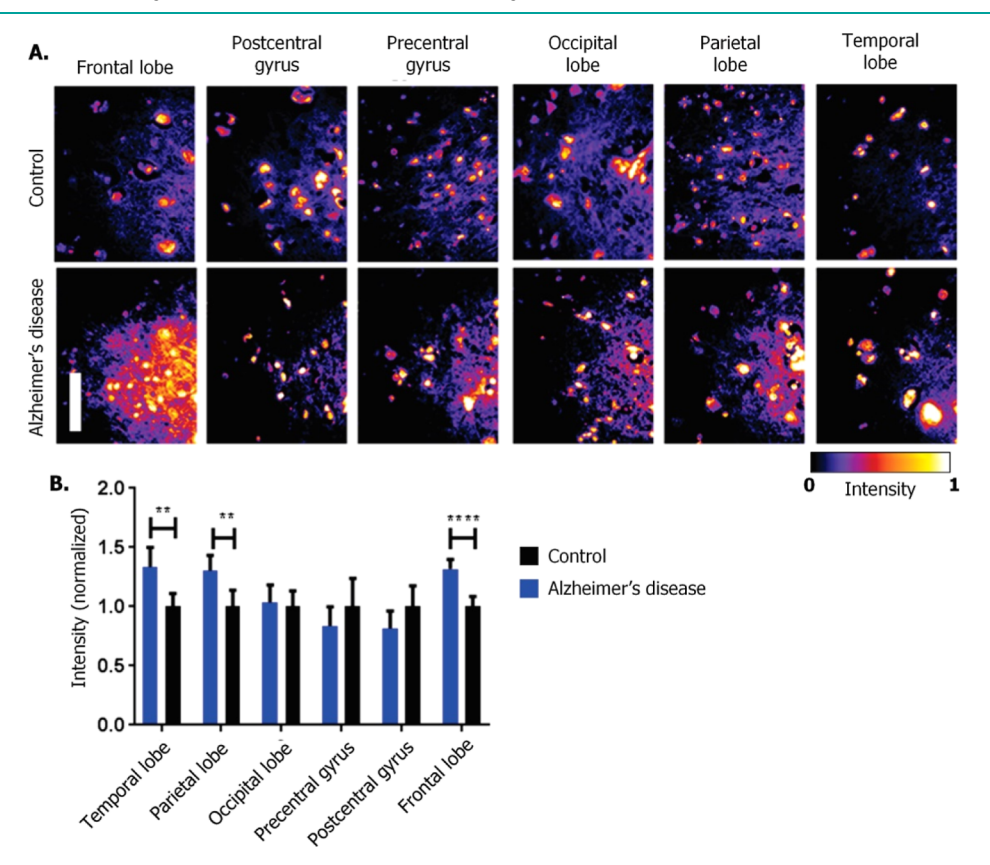


Figure 5. Hematoxylin NIR emission in human tumor tissue samples. (A) Representative images of human cancer samples co-stained with SOD-1 DAB-IHC and H&E (scalebar =  $100 \ \mu m$ ). (B) Representative broadband NIR images of a high-positive SOD-1 region and a low-positive SOD-1 region with false-color added to show normalized intensity. Scale bar =  $30 \ \mu m$ . (C) Normalized intensity of hematoxylin NIR emission from healthy control, low-SOD-1, and high-SOD-1 DAB-IHC stained samples grouped by tissue type (N = 648).



**Figure 6.** Hematoxylin NIR emission in AD tissue samples. (A) Representative broadband NIR images of AD samples and matched healthy controls; false-color was added to report normalized intensity (scalebar =  $30 \mu m$ ). (B) Normalized intensity of hematoxylin NIR emission from AD brain regions in diseased samples and matched healthy controls (N = 215).

samples, the preservation of this response in brain regions suggests that ferritin may play a protective role against oxidative stress. Clinically, the NIR emission of hematoxylin may lend clinical insight into these conditions or others where oxidative stress is an important marker of disease or treatment

progression.<sup>23–28</sup> This analysis has the added benefit of not requiring additional steps or processing, as it is immediately accessible from the ubiquitous H&E stain.

### CONCLUSIONS

Herein, we describe previously unreported NIR spectral properties from the hematoxylin nuclear stain, consisting of an emission tail in NIR-II. This emission is dependent on mordant, with Fe(III) hematoxylin showing absorbance peak broadening and stronger emission than Al(III) hematoxylin. The NIR emission peak of Al(III) hematoxylin, the formulation most commonly used in the H&E staining, is responsive to endogenous Fe(III) trafficking, with increased Fe(III) availability producing an increase in emission intensity. These findings are consistent with endogenous Fe(III) having the capacity to serve as a mordant to the hematoxylin stain in addition to, or replacing, the original Al(III) mordant. Furthermore, Al(III) hematoxylin NIR emission was responsive to H2O2-induced oxidative stress in cell samples, and this response was dependent on nuclear translocation of the major iron transport protein ferritin, consistent with the essential role of iron-coordination and not direct dye-oxidation. This hematoxylin emission response is preserved in samples of human tumor and AD samples compared to matched tissue controls. In human cancer tissue, we found that hematoxylin emission intensity correlated with the oxidative stress marker SOD-1. Further investigations of the structure of the active emissive agent and the potential of developing a ratiometric analysis based on the emission properties of the hematoxylin stain are of great interest for future research. These results portend the potential use of the hematoxylin stain to probe the presence of oxidative stress, via nuclear translocation of ferritin in samples of clinical interest.

#### ASSOCIATED CONTENT

# **Solution** Supporting Information

The Supporting Information is available free of charge at https://pubs.acs.org/doi/10.1021/acschembio.3c00156.

Data include NIR spectral analysis of H&E-stained live cells and tissue samples, absorbance spectra of hematoxylin solution with mordants, absorbance spectra change of hematein and hematoxylin at varying pH and oxidation state or in presence of Fe(III) and gDNA, IF staining of ferritin, and NIR spectral analysis of H&E-stained cells with Al(III) or Fe(III) mordants (PDF).

## AUTHOR INFORMATION

## **Corresponding Author**

Daniel A. Heller — Weill Cornell Medicine, Cornell University, New York, New York 10065, United States; Memorial Sloan Kettering Cancer Center, New York, New York 10065, United States; occid.org/0000-0002-6866-0000; Email: hellerd@mskcc.org

#### Authors

Rachel E. Langenbacher — Weill Cornell Medicine, Cornell University, New York, New York 10065, United States Christopher P. Horoszko — Memorial Sloan Kettering Cancer Center, New York, New York 10065, United States;
ocid.org/0000-0003-2344-4707

Mijin Kim – Memorial Sloan Kettering Cancer Center, New York, New York 10065, United States; orcid.org/0000-0002-7781-9466

Complete contact information is available at: https://pubs.acs.org/10.1021/acschembio.3c00156

#### **Author Contributions**

All authors contributed to the final manuscript and approved the final version.

### **Funding**

This work was supported in part by the National Science Foundation CAREER Award (1752506), the NCI (R01-CA215719 and the Cancer Center Support Grant, P30-CA008748), the American Cancer Society Research Scholar Grant (GC230452), the Pershing Square Sohn Cancer Research Alliance, the Honorable Tina Brozman Foundation for Ovarian Cancer Research, the Ara Parseghian Medical Research Fund, the Louis and Rachel Rudin Foundation, the Expect Miracles Foundation—Financial Services Against Cancer, the Anna Fuller Fund, Mr. William H. Goodwin and Mrs. Alice Goodwin and the Commonwealth Foundation for Cancer Research, the Experimental Therapeutics Center, and the Center for Molecular Imaging and Nanotechnology of Memorial Sloan Kettering Cancer Center. R.L. and C.H. were supported by an NIH T32 training grant (T32-GM73546). M.K. was supported by the NIH (K99-EB033580) and Marie-Josée Kravis Women in Science Endeavor Postdoctoral Fellowship.

#### Notes

The authors declare the following competing financial interest(s): D.A.H. is a co-founder and officer with equity interest in Lime Therapeutics, Inc., a cofounder with equity interest in Selectin Therapeutics, Inc., and Resident Diagnostics, Inc., and a member of the scientific advisory board of Concarlo Therapeutics, Inc., Nanorobotics, Inc., and Mediphage Bioceuticals, Inc.

#### ACKNOWLEDGMENTS

We would like to thank MSK Molecular Cytology Core Facility for IF staining, confocal microscopy imaging, and image analysis.

# REFERENCES

- (1) Naik, N.; Madani, A.; Esteva, A.; Keskar, N. S.; Press, M. F.; Ruderman, D.; Agus, D. B.; Socher, R. Deep Learning-Enabled Breast Cancer Hormonal Receptor Status Determination from Base-Level H&E Stains. *Nat. Commun.* **2020**, *11*, 5727.
- (2) Gibbs, S. L.; Genega, E.; Salemi, J.; Kianzad, V.; Goodwill, H. L.; Xie, Y.; Oketokoun, R.; Khurd, P.; Kamen, A.; Frangioni, J. v. Near-Infrared Fluorescent Digital Pathology for the Automation of Disease Diagnosis and Biomarker Assessment. *Mol. Imag.* 2015, 14, 7290.
- (3) Kiernan, J. A. Does progressive nuclear staining with hemalum (alum hematoxylin) involve DNA, and what is the nature of the dyechromatin complex? *Biotech. Histochem.* **2018**, *93*, 133.
- (4) Thompson, K. J.; Fried, M. G.; Ye, Z.; Boyer, P.; Connor, J. R. Regulation, Mechanisms and Proposed Function of ferritin Translocation to Cell Nuclei. *J. Cell Sci.* **2002**, *115*, 2165–2177.
- (5) Yi, X. M.; Wang, F. L.; Qin, W. J.; Yang, X. J.; Yuan, J. L. Near-Infrared Fluorescent Probes in Cancer Imaging and Therapy: An Emerging Field. *Int. J. Nanomed.* **2014**, *9*, 1347–1365.
- (6) Tuer, A.; Tokarz, D.; Prent, N.; Cisek, R.; Alami, J.; Dumont, D. J.; Bakueva, L.; Rowlands, J. A.; Barzda, V. Nonlinear Multicontrast Microscopy of Hematoxylin-and-Eosin-Stained Histological Sections. *J. Biomed. Opt.* **2010**, *15*, 1.
- (7) True, L. D.; Gao, X. Quantum Dots for Molecular Pathology: Their Time Has Arrived. *J. Mol. Diagn.* **2007**, *9*, 7–11.
- (8) Gibbs, S. L.; Genega, E.; Salemi, J.; Kianzad, V.; Goodwill, H. L.; Xie, Y.; Oketokoun, R.; Khurd, P.; Kamen, A.; Frangioni, J. v. Near-Infrared Fluorescent Digital Pathology for the Automation of Disease Diagnosis and Biomarker Assessment. *Mol. Imag.* 2015, 14, 7290.

- (9) Cahill, L. C.; Giacomelli, M. G.; Yoshitake, T.; Vardeh, H.; Faulkner-Jones, B. E.; Connolly, J. L.; Sun, C. K.; Fujimoto, J. G. Rapid Virtual Hematoxylin and Eosin Histology of Breast Tissue Specimens Using a Compact Fluorescence Nonlinear Microscope. *Lab. Invest.* **2018**, *98*, 150–160.
- (10) Manley, M. Near-Infrared Spectroscopy and Hyperspectral Imaging: Non-Destructive Analysis of Biological Materials. *Chem. Soc. Rev.* **2014**, *43*, 8200–8214.
- (11) Roxbury, D.; Jena, P. v.; Williams, R. M.; Enyedi, B.; Niethammer, P.; Marcet, S.; Verhaegen, M.; Blais-Ouellette, S.; Heller, D. A. Hyperspectral Microscopy of Near-Infrared Fluorescence Enables 17-Chirality Carbon Nanotube Imaging. *Sci. Rep.* **2015**, 5, 14167.
- (12) Surguladze, N.; Patton, S.; Cozzi, A.; Fried, M. G.; Connor, J. R. Characterization of Nuclear Ferritin and Mechanism of Translocation. *Biochem. J.* **2005**, 388, 731–740.
- (13) Jo, T. G.; Jung, J. M.; Han, J.; Lim, M. H.; Kim, C. A Single Fluorescent Chemosensor for Multiple Targets of Cu2+, Fe2+/3+ and Al3+ in Living Cells and a near-Perfect Aqueous Solution. *RSC Adv.* **2017**, *7*, 28723–28732.
- (14) Kim, N. H.; Lee, J.; Park, S.; Jung, J.; Kim, D. A Schiff Base Fluorescence Enhancement Probe for Fe(III) and Its Sensing Applications in Cancer Cells. *Sensors* **2019**, *19*, 2500.
- (15) Liu, Y.; Liu, C.; Zhang, X.; Liu, L.; Ge, C.; Zhuang, X.; Zhang, N.; Yang, Q.; Huang, Y. Q.; Zhang, Z. Highly Selective and Sensitive Detection of Fe 3+, Al 3+ and Picric Acid by a Water-Stable Luminescent MOF. *J. Solid State Chem.* **2019**, 272, 1–8.
- (16) Maity, K.; Mukherjee, D.; Sen, M.; Biradha, K. Fluorescent Dye-Based Metal-Organic Framework Piezochromic and Multicolor-Emitting Two-Dimensional Materials for Light-Emitting Devices. *ACS Appl. Nano Mater.* **2019**, *2*, 1614–1620.
- (17) Bruner, E.; Jacobs, H. I. Alzheimer's Disease: The Downside of a Highly Evolved Parietal Lobe? *J. Alzheimer's Dis.* **2013**, *35*, 227–240.
- (18) Killiany, R. J.; Moss, M. B.; Albert, M. S.; Sandor, T.; Tieman, J.; Jolesz, F. Temporal Lobe Regions on Magnetic Resonance Imaging Identify Patients with Early Alzheimer's Disease. *Arch. Neurol.* **1993**, 50, 949–954.
- (19) Scharre, D. W.; Weichart, E.; Nielson, D.; Zhang, J.; Agrawal, P.; Sederberg, P. B.; Knopp, M. v.; Rezai, A. R. Deep Brain Stimulation of Frontal Lobe Networks to Treat Alzheimer's Disease. *J. Alzheimer's Dis.* **2018**, *62*, *621*–*633*.
- (20) Murakami, K.; Murata, N.; Noda, Y.; Tahara, S.; Kaneko, T.; Kinoshita, N.; Hatsuta, H.; Murayama, S.; Barnham, K. J.; Irie, K.; Shirasawa, T.; Shimizu, T. SOD1 (Copper/Zinc Superoxide Dismutase) Deficiency Drives Amyloid  $\beta$  Protein Oligomerization and Memory Loss in Mouse Model of Alzheimer Disease. *J. Biol. Chem.* **2011**, 286, 44557–44568.
- (21) Mota, S. I.; Costa, R. O.; Ferreira, I. L.; Santana, I.; Caldeira, G. L.; Padovano, C.; Fonseca, A. C.; Baldeiras, I.; Cunha, C.; Letra, L.; Oliveira, C. R.; Pereira, C. M. F.; Rego, A. C. Oxidative Stress Involving Changes in Nrf2 and ER Stress in Early Stages of Alzheimer's Disease. *Biochim. Biophys. Acta, Mol. Basis Dis.* **2015**, 1852, 1428–1441.
- (22) Ayton, S.; Faux, N. G.; Bush, A. I.; Weiner, M. W.; Aisen, P.; Petersen, R.; Jack, C. R.; Jagust, W.; Trojanowki, J. Q.; Toga, A. W.; et al. Ferritin Levels in the Cerebrospinal Fluid Predict Alzheimer's Disease Outcomes and Are Regulated by APOE. *Nat. Commun.* **2015**, *6*, 6760.
- (23) Hayes, J. D.; Dinkova-Kostova, A. T.; Tew, K. D. Oxidative Stress in Cancer. Cancer Cell 2020, 38, 167–197.
- (24) Salatino, A.; Aversa, I.; Battaglia, A. M.; Sacco, A.; di Vito, A.; Santamaria, G.; Chirillo, R.; Veltri, P.; Tradigo, G.; di Cello, A.; Venturella, R.; Biamonte, F.; Costanzo, F. H-Ferritin Affects Cisplatin-Induced Cytotoxicity in Ovarian Cancer Cells through the Modulation of ROS. Oxid. Med. Cell. Longev. 2019, 2019, 1–13.
- (25) Carocci, A.; Catalano, A.; Sinicropi, M. S.; Genchi, G. Oxidative Stress and Neurodegeneration: The Involvement of Iron. *BioMetals* **2018**, *31*, 715–735.

- (26) Levenson, C. W.; Tassabehji, N. M. Iron and Ageing: An Introduction to Iron Regulatory Mechanisms. *Aging Res. Rev.* **2004**, *3*, 251–263.
- (27) Forman, H. J.; Zhang, H. Targeting Oxidative Stress in Disease: Promise and Limitations of Antioxidant Therapy. *Nat. Rev. Drug Discovery* **2021**, *20*, 689–709.
- (28) Waalen, J.; Felitti, V. J.; Gelbart, T.; Beutler, E. Screening for Hemochromatosis by Measuring Ferritin Levels: A More Effective Approach. *Blood* **2008**, *111*, 3373–3376.